Monthly Notices
of the
ROYAL ASTRONOMICAL SOCIETY

MNRAS **460,** 1999–2007 (2016)
Advance Access publication 2016 April 21

doi:10.1093/mnras/stw923

Spectroscopic study of the HgMn star HD 49606: the quest for binarity, abundance stratifications and magnetic field

G. Catanzaro,[1]★ M. Giarrusso,[2,1] F. Leone,[2,1] M. Munari,[1] C. Scalia,[2,1] E. Sparacello[2] and S. Scuderi[1]

[1]*INAF – Osservatorio Astrofisico di Catania, Via S.Sofia 78, I-95123 Catania, Italy*
[2]*Università degli studi di Catania, Via S.Sofia 78, I-95123 Catania, Italy*

Accepted 2016 April 18. Received 2016 April 18; in original form 2016 February 16

ABSTRACT

In this paper, we present a multi-instrument analysis of the mercury-manganese star HD 49606. New spectroscopic observations have been obtained by us with Catania Astrophysical Observatory Spectropolarimeter (CAOS@OAC) and High Accuracy Radial Velocity Planet Searcher-North@Telescopio Nazionale Galileo (HARPS-N@TNG). Combining these observations with archive data coming from other instruments, we performed a comprehensive analysis of this star. We highlight the motion around the centre of mass of a binary system of SB1 type, and we calculate the fundamental parameters characterizing its orbit. We also speculate on the nature of the unseen component. From the fit of H β and H γ, we determined the effective temperature and gravity, while from a number of metal lines, we derive the rotational and microturbulent velocities. Regarding chemical composition, we found underabundances of helium, oxygen, magnesium, sulfur and nickel, solar composition for carbon and overabundances for all the other elements. In particular, mercury abundance is derived taking into account an isotopic mixture different from the terrestrial one. As to magnesium, silicon and phosphorus, we found a non-constant abundance with the optical depth, a result currently considered an evidence of stratification. Spectropolarimetric observations have been performed in the attempt to highlight the presence of a magnetic field, but no detection has been found.

Key words: stars: abundances – binaries: spectroscopic – stars: chemically peculiar – stars: early-type – stars: individual: HD 49606.

1 INTRODUCTION

Mercury-manganese stars, or HgMn stars, are main-sequence objects with effective temperatures ranging in the interval between 10 000 and 15 000 K. They belong to the third group of chemically peculiar stars (CP3) as defined by Preston (1974). Compared with the Sun, they are characterized by strong overabundances of mercury (up to 6 dex) and manganese (up to 3 dex) and large underabundance of helium, among others.

To explain these anomalies in their atmospheres, radiatively driven selective diffusion is mostly invoked (Michaud 1970; Alecian & Stift 2002). This phenomenon could be favoured by the quiet atmospheres, since they do not have a convective zone and rotate slowly compared to normal late-B stars. Moreover, HgMn stars present a high rate of binarity (Smith 1996). A natural consequence of diffusion is the presence of inhomogeneities in the vertical distribution of chemical abundances (Vauclair 1975; Alecian & Stift 2002; Stift & Alecian 2016).

HD 49606 (=HIP 32753 = OV Gem = 33 Gem) has been classified as a star with spectral peculiarity of the Am type by Garrison & Gray (1994), who gave a full spectral classification of kB8hB7HeB9.5 IV-V. The authors gave also an indication of a possible peculiarity of HgMn class. This object has been definitively classified as an HgMn star in the Catalogue of Ap, HgMn and Am stars by Renson, Gerbaldi & Catalano (1991).

Photometric observations of HD 49606 were performed by Chunakova, Bychov & Glagolevskii (1981), who found the light variations to occur with a period of 3.099 d, and by Glagolevskij, Panov & Chunakova (1985), who found two possible period values, namely 3.3546 d and 1.418 64 d. Recently, by using data from STEREO satellite, Paunzen et al. (2013) found this star being photometrically variable with a period of 2.266 10 ± 0.002 40 d. From the spectroscopic point of view, variability has been searched for by Catanzaro, Leone & Catalano (1999) who found constancy for what that concerns the equivalent width of the He I λ5876 Å.

HD 49606 is an HgMn star of special interest for a number of reasons, first of all, the controversial presence of an unseen companion. Stickland & Weatherby (1984) concluded that this object is probably constant in radial velocity, and also Schöeller et al. (2010) in their

★ E-mail: gca@oact.inaf.it

NACO@VLT survey of 56 HgMn stars did not resolve any companion, while the presence of an optical component of magnitude 13.3 at a distance of 27.5 arcsec is mentioned by Lindroos (1985). Nevertheless, McDonald, Zijlstra & Boyer (2012) found evidence of infrared (IR) excess that could be explained with the presence of a secondary component cooler than the primary. The binarity is suggested also by Savanov & Hubrig (2003) to explain the tendency of the spectral lines observed in their spectrum to be rectangular, interpreted as an incipient separation in two components.

Moreover, this star has been investigated by the same authors, paying particular attention to the stratification of chromium. They studied a sample of 10 HgMn, and they did not find evidence of stratification only in HD 49606.

Also the presence of a magnetic field is controversial, Glagolevskij et al. (1985) observed a strong longitudinal magnetic field (1.4 ± 0.1 kG), that was not confirmed later by Hubrig & Launhardt (1993). Later on, Hubrig et al. (2006) in their Catalogue of magnetic field measurements with FORS 1 at the VLT, reported a longitudinal magnetic field of −11 ± 71 G.

The aim of this paper is to present our new results on the spectroscopic binary nature of HD 49606 and on the vertical stratification of some chemical elements. These purposes have been achieved by using both new spectroscopic observations and analysing archived data from ESO. Moreover, we performed circular spectropolarimetry with CAOS@OAC to find evidence of a magnetic field.

2 OBSERVATIONS AND DATA REDUCTION

To investigate the possible binary nature of HD 49606, time-resolved spectroscopy was carried out at the Catania Astrophysical Observatory Spectropolarimeter (CAOS) which is a fibre-fed, high-resolution, cross-dispersed echelle spectrograph (Spanò et al. 2004, 2006; Catanzaro et al. 2015; Leone et al. 2016) recently installed at the Cassegrain focus of the 91 cm telescope of the 'M. G. Fracastoro' observing station of the Catania Astrophysical Observatory (Mt. Etna, Italy). A number of 18 spectra were obtained in 2014 and in 2015 with exposure times ranging from 1200 to 1800 s, the signal-to-noise ratio was at least 100 in the continuum in the 3900–8000 Å wavelength range, with a resolution of $R = 45\,000$, as measured from ThAr and telluric lines. Further, the 2.1 m telescope of the Complejo Astronomico El Leoncito, equipped with a Boller & Chivens Cassegrain spectrograph, has been used to collect six spectra in 1995 December (see Leone, Catalano & Malaroda 1997).

We observed HD 49606 with other instruments, one spectrum with High Accuracy Radial Velocity Planet Searcher-North@Telescopio Nazionale Galileo (HARPS-N@TNG) and two spectra with FRESCO@OAC (see Catanzaro & Leto 2004, for detail). We also used archive data, in particular: one observed with CES@3.6 metre telescope, one with the New Technology Telescope (NTT) equipped with the ESO MultiMode Instrument (EMMI), and one from the f/4 coudé spectrograph Gecko@CFHT. Description of these data are reported in Table 1.

The reduction of all spectra, which included the subtraction of the bias frame, trimming, correcting for the flat-field and the scattered light, extraction for the orders, and wavelength calibration, was done using the NOAO/IRAF packages.[1]

The IRAF package RVCORRECT was used to determine the heliocentric velocity correcting the spectra for the Earth's motion.

[1] IRAF is distributed by the National Optical Astronomy Observatory, which is operated by the Association of Universities for Research in Astronomy, Inc.

Table 1. Brief summary of our spectra: spectrograph and telescope, spectral range, resolving power, maximum signal to noise obtained.

Instrument	Range (Å)	$R = \frac{\lambda}{\Delta\lambda}$	SNR
CAOS@OAC[a]	3900–8000	45 000	100
HARPS-N@TNG[b]	3900–6900	115 000	200
B&C@CASLEO	4000–7000	26 000	250
FRESCO@OAC	4810–5370	14 000	100
CES@ESO3.6	6125–6165	164 000	270
EMMI@NTT	3970–6620	60 000	500
Gecko@CFHT	4420–4490	85 000	600

Notes. [a]Leone et al. (2016).
[b]Cosentino et al. (2012).

3 ATMOSPHERIC PARAMETERS

In B-type stars, Balmer lines profiles are sensitive both to effective temperature and surface gravity. For the analysis of Balmer lines, we used the EMMI@NTT spectrum, since it is the one with the highest spectral resolution and signal-to-noise ratio. The approach we used in this paper was to minimize the difference between observed and synthetic H β and H γ profiles. As goodness-of-fit test, we used the parameter

$$\chi^2 = \frac{1}{N}\sum\left(\frac{I_{\rm obs}-I_{\rm th}}{\delta I_{\rm obs}}\right)^2,$$

where N is the total number of points, $I_{\rm obs}$ and $I_{\rm th}$ are the intensities of the observed and computed profiles, respectively, and $\delta I_{\rm obs}$ is the photon noise.

Atmospheric models obtained with ATLAS9 (Kurucz 1993a) use pre-computed line opacities in the form of opacity distribution functions, that are tabulated for multiples of the solar metallicity and for various microturbulent velocities (Kurucz 1993b). This approach allows very fast computation of model atmospheres, but with very little flexibility in the choice of chemical profile and microturbulent velocity. While this is satisfactory for most applications, it could fail for chemically peculiar stars where a non-solar chemical composition is required. This problem can be overcome with ATLAS12 (Kurucz 1997), which is essentially identical to ATLAS9, but uses the opacity sampling method to evaluate line opacities.

As starting values of $T_{\rm eff}$, we used the value derived from Strömgren photometry: $b - y = -0.057 \pm 0.001$, $m_1 = 0.111 \pm 0.005$, $c_1 = 0.500 \pm 0.010$, $\beta = 2.702 \pm 0.001$ (Hauck & Mermilliod 1998). Using these values, the calibration of Moon & Dworetsky (1985) leads to $T_{\rm eff} = 14\,590$ K. Note, however, that because of increased line blanketing in peculiar stars and consequent flux redistribution (Leone & Catalano 1991), these must be taken merely as provisional values.

The fitting of H β and H γ profiles were generated in three steps: first, we computed the stellar atmosphere model for solar chemical abundances by using the ATLAS9 code (Kurucz 1993a), then stellar spectrum was synthesized using SYNTHE (Kurucz & Avrett 1981) and finally, the instrumental and rotational broadening were applied. This procedure gave

$$T_{\rm eff} = 12\,900 \pm 150\,{\rm K} \text{ and } \log g = 3.60 \pm 0.05.$$

These values are lower than those reported in the literature at least 800 K and 0.15 dex, respectively (Dworetsky, Persaud & Patel 2008; Netopil et al. 2008).

The microturbulent velocity ξ, has been determined from 30 Fe II lines with equivalent width EW > 10 mÅ. In particular, ξ has been computed by requiring that the derived abundances do not depend on the measured equivalent widths. To convert equivalent widths to

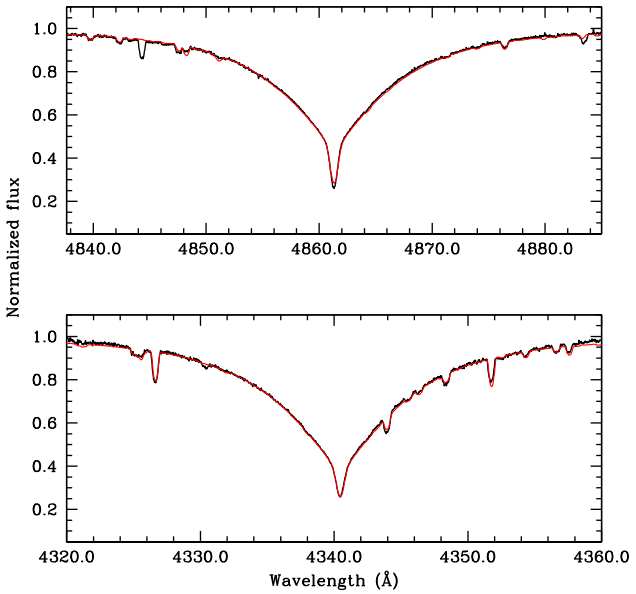

Figure 1. Comparison between observed and computed H β and H γ profiles, computed by ATLAS12 and SYNTHE as explained in the text.

abundances, we used the WIDTH9 code (Kurucz & Avrett 1981). The adopted microturbulence is $\xi = 0.3^{+0.9}_{-0.0}$ km s^{-1}.

To measure the $v_e \sin i$ of HD 49606, we took advantage from the highest resolving power spectrum at our disposal, i.e. the $R = 164\,000$ CES spectrum. By matching synthetic line profiles from SYNTHE to a number of metal lines, the best fit was obtained with $v_e \sin i = 19.0 \pm 0.5$ km s^{-1}. This value is in agreement with $v_e \sin i = 20$ km s^{-1} reported by Abt, Levato & Grosso (2002).

By using these atmospheric parameters, we derived helium and metals abundances by spectral synthesis. A first look at helium lines reveals an extreme underabundance for this element, as expected for HgMn stars, since diffusion theory predicts that the photospheres of all HgMn stars should be deficient in helium, which was confirmed for instance in a dedicated study by Dworetsky (2004). Because of such deficiency, the abundances based on ATLAS9 model were used as input data for an ATLAS12 model, and we used this new model to refine the fitting of Balmer lines. A search for an appropriate ATLAS12 model suitable to reproduce the Balmer line profile has finally yielded

$$T_{\rm eff} = 13\,000 \pm 150\,{\rm K} \text{ and } \log g = 3.80 \pm 0.05.$$

In Fig. 1, we show the comparison between observed and computed H β and H γ profiles. Derived $T_{\rm eff}$ and $\log g$ values are in agreement with the results by Catanzaro et al. (1999), at least within errors.

The importance of a correct assumption of helium abundance has been already investigated by Leone & Manfrè (1997) and Catanzaro, Leone & Dall (2004) for a sample of helium-weak stars. The result shared by those papers is that neglecting the correct helium abundance the effective temperature can be underestimated up to 7 per cent and the $\log g$ can be underestimated up to 0.25 dex. As to HD 49606, we can confirm this result for what concerns the gravity, but nothing we can conclude for the effective temperature, since the difference is within the experimental errors.

Table 2. Heliocentric Julian Date and measured radial velocities for HD 49606.

	HJD (2400000.0 +)	RV (km s^{-1})
CASLEO	50057.78573	7.52 ± 1.29
	50058.75608	4.51 ± 0.36
	50060.78595	5.06 ± 0.46
	50061.81615	0.68 ± 0.50
	50062.77233	6.61 ± 0.55
	50063.76100	5.82 ± 0.36
EMMI	51252.51598	6.73 ± 0.51
FRESCO	52221.62576	10.19 ± 0.40
	52235.59984	9.00 ± 0.25
CES	52299.72530	10.03 ± 0.07
CFHT	53102.75640	11.83 ± 0.68
CAOS	56737.33238	7.71 ± 0.67
	56747.30886	8.78 ± 0.45
	57130.26629	9.09 ± 0.37
	57131.28842	10.46 ± 0.66
	57278.61732	8.33 ± 0.44
	57279.62338	6.94 ± 0.43
	57282.61732	8.72 ± 0.45
	57283.60942	7.43 ± 0.44
	57290.65282	6.01 ± 1.66
	57307.53853	7.38 ± 0.59
	57330.64252	9.40 ± 0.82
	57331.46733	7.59 ± 0.43
	57332.59994	7.14 ± 0.56
	57336.54988	9.78 ± 0.42
	57337.45853	6.33 ± 0.44
	57339.63108	11.51 ± 0.49
	57340.56566	9.70 ± 0.71
	57346.53371	10.99 ± 0.40
HARPS-N	57340.61110	10.07 ± 0.07

4 THE DETERMINATION OF ORBITAL PARAMETERS

The radial velocities for a spectroscopic binary system are given from the following equation:

$$V_{\rm rad} = \gamma + K[\cos(\theta + \omega) + e\cos\omega], \quad (1)$$

where γ is the radial velocity of the centre of mass, e is the eccentricity of the orbit, ω is the longitude of the periastron, θ is the angular position of the star measured from the centre of mass at a given instant and K is the semi-amplitude of the velocity curve as given by the formula:

$$K = \frac{2\pi a \sin i}{P\sqrt{1-e^2}}, \quad (2)$$

where P is the orbital period of the system, a is the semimajor axis and i is the inclination angle.

Radial velocity measurements of HD 49606 have been reported by Stickland & Weatherby (1984) and by Aikman (1976).

The radial velocities reported in Table 2 have been measured by cross-correlating the observed spectra with the one observed by HARPS-N. The cross-correlation has been calculated by *fxcor* IRAF package, paying particular attention in excluding Balmer lines from the correlation, as well intervals with telluric lines.

By using velocities derived from our spectra, orbital elements have been determined by a weighted least-squares fitting to equation (1). Errors have been estimated as the variation in the

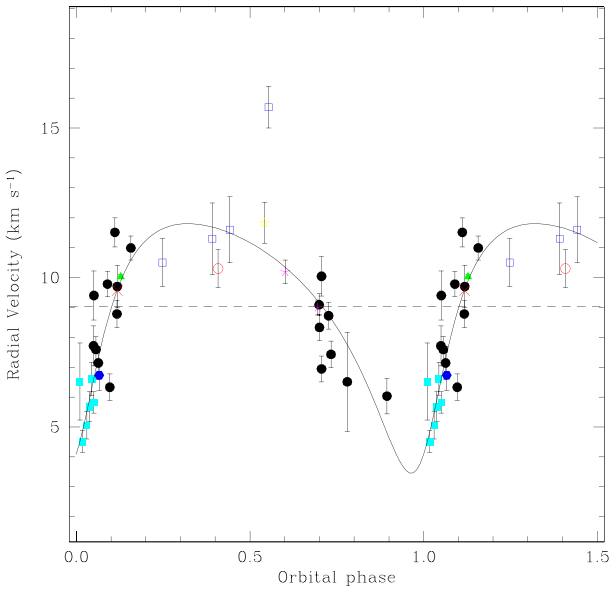

Figure 2. Radial velocity curve for HD 49606. Meaning of the symbols is: black dots represent radial velocities from CAOS@OAC, green triangles from CES@ESO, yellow hexagon from EMMI@NTT, cyan boxes from CASLEO, magenta asterisks from FRESCO@OAC and star symbol for CFHT. Literature values are plotted as well with the following symbols: open red circle for Aikman (1976) and open blue square for Stickland & Weatherby (1984) data. Error bars are as large as 1σ's.

parameters which increases the χ^2 of a unit. We obtained the following solution:

P: 148.30 ± 0.04 d
T: $2457\,471.517 \pm 0.246$
e: 0.40 ± 0.01
ω: $212^\circ \pm 1^\circ$
K: 4.2 ± 0.4 km s^{-1}
γ: 9.04 ± 0.05 km s^{-1}
$a \sin i$: 11.2 ± 1.1 R$_\odot$
$f(m)$: $(8.6 \pm 2.5) \cdot 10^{-4}$ M$_\odot$

where the mass function $f(m)$ is defined as

$$f(m) = \left(\frac{M_2}{M_1 + M_2}\right)^2 M_2 \sin^3 i \qquad (3)$$

This solution has been overplotted on the measured velocities in Fig. 2.

Regarding the secondary component, we do not find any spectral signature, thus we can only speculate about the possible nature of this unseen object.

Paunzen et al. (2013) estimated a mass of $M = 4.45 \pm 0.28$ M$_\odot$, while Pasinetti Fracassini et al. (2001) report in their CADARS catalogue a value for the radius $R = 4.2$ R$_\odot$. According to Drilling & Landolt (1999), these values of mass and radius are compatible with a main-sequence star having the effective temperature and gravity we adopted (see Section 3).

Using the relation:

$$v \sin i = 50.6 \frac{R_* \sin i}{P}, \qquad (4)$$

(where i is the angle between the rotational axis and the line of sight, R_* is the stellar radius in solar radii, velocities are in km s^{-1} and P is the rotational period expressed in days), we derived an inclination angle $i \approx 12^\circ$, using the $v \sin i = 19$ km s^{-1} derived by us (see Section 3), the rotational period given by Paunzen et al. (2013) and

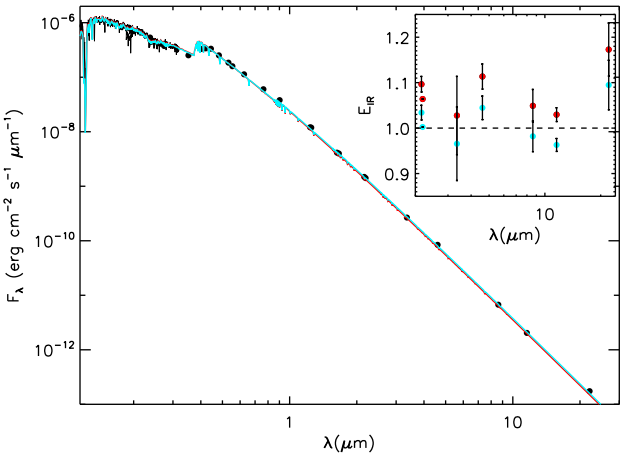

Figure 3. SED observed for HD 49606, photometric sources collected to build the distribution are: IUE satellite (solid thin curve), Jamar et al. (1976, solid thick line) Spectrophotometric observation, TD1 satellite (Thompson et al. 1978), Johnson BVJHK (Anderson & Francis 2012), 2MASS, SDSS, HIP: VT,BT (Pickles & Depagne 2010), HIP: Hp (Van Leeuven 2007), AKARI (Ishishara et al. 2010), and *WISE* (Wright et al. 2010). We overimposed two theoretical models computed by means of ATLAS9 both for single (red solid line) and composite (blue dashed line) spectrum, as described in the text. In the inset, we plotted the infrared excess computed as described in the text both for single and composite spectrum.

the radius derived by Pasinetti Fracassini et al. (2001). Assuming that the rotational axis of HD 49606 is perpendicular to the orbital plane, we estimated the mass of the companion. For the value of $M_1 = 4.45$ M$_\odot$ and $i \approx 12^\circ$, inverting equation (3), we obtained $M_2 = 1.55 \pm 0.20$ M$_\odot$, which corresponds to a star of spectral type of F1V and a radius $R_2 = 1.45 \pm 0.16$ R$_\odot$.

Given the small amplitude of the curve, we investigated also the possibility that the variability of observed radial velocity could be due not to an orbital motion but to periodic visibility of chemical inhomogeneities on the surface modulated by the stellar rotation. Nevertheless, three aspects convinced ourselves that the observed radial velocities variations are effectively due to an orbital motion caused by the presence of a cooler unseen companion. First of all, hydrogen lines do not show any significant modulation in their radial velocity. In slowly rotating B-type stars, the hydrogen lines have broad wings and sharp cores. For our purpose, while the wings are useless since they can be affected by different spectral lines, the sharp cores do not suffer of this contamination and the flux is formed in the upper layers of the atmosphere. As a check, when possible, we computed the radial velocities from H α and H β cores and we found an average discrepancy with respect to metal lines of $\approx$0.28 km s^{-1}. In addition, by using the EMMI spectrum, we measured the radial velocities from all phosphorus and silicon lines separately, obtaining the same values within the experimental errors.

Moreover, the hypothesis of a cooler companion, is consistent with the presence of an IR excess. Following McDonald et al. (2012), we defined the IR excess as

$$E_{\rm IR} = \frac{1}{n} \sum_{\lambda > 2\mu} \frac{F_{\rm o}}{F_{\rm t}}, \qquad (5)$$

where n is the number of points, $F_{\rm o}$ is the observed flux and $F_{\rm t}$ is the corresponding theoretical one. In Fig. 3, we compared the observed spectral energy distribution (SED) of HD 49606 with theoretical fluxes computed by using ATLAS9 (Kurucz & Avrett 1981). Since the star is relatively close to the Earth (D = 263 ± 29 pc;

Van Leeuven 2007), and the colour excess $E(B-V) = -0.01$ (Jamar et al. 1976), we decide to not deredden the flux distribution. The red solid line represents the model computed with the parameters derived in Section 3, for which we obtained $E_{IR} = 1.09 \pm 0.04$, consistent with McDonald et al. (2012) value. The dashed blue line represents the model obtained combining the fluxes of the primary and of a F1V secondary component. In this case, the E_{IR} decrease to a value of 1.00 ± 0.04.

Finally, in a review concerning the binarity among Bp–Ap stars, Gerbaldi, Floquet & Hauck (1985) pointed out that the period–eccentricity distribution for HgMn stars shows the existence of a slightly bimodal distribution for $0.4 < e < 0.5$, which is less present in the normal star sample. This result has been confirmed later on by Catanzaro & Leto (2004). Our values of orbital period and eccentricity of HD 49606 are in agreement with this distribution, at least within the experimental errors.

5 ABUNDANCES

For abundances determination, we used the following spectra.

(i) EMMI@NTT because of its highest value of signal-to-noise ratio, in the spectral region up to λ 6620 Å;
(ii) CAOS@OAC spectra to analyse spectral features at the longest wavelengths;
(iii) HARPS-N@TNG for the spectral region containing the Hg II λ 3984 Å, at the highest spectral resolution and S/N.

To derive the abundances of individual species, we divided our spectra into several intervals, 50 Å wide each, and derived the abundances in every interval by performing a χ^2 minimization of the difference between the observed and the synthetic spectrum. The minimization algorithm has been written in IDL[2] language, using the *amoeba* routine. We adopted lists of spectral lines and atomic parameters from Castelli & Hubrig (2004), who updated the parameters listed originally by Kurucz & Bell (1995).

In the following analysis, we neglected the presence of the secondary component since the radii ratio is very low ($R_2/R_1 \approx 0.34$) and the impact of the flux coming from the unseen companion does not affect the total observed flux. As an example, we show in Fig. 4, a comparison between observed and synthetic spectra in the region containing, among other, Fe II λλ 4508.288, 4515.339, 4520.224, and 4522.634 and Mn II λ 4518.9 Å.

For each element reported in Table 3 and plotted in Fig. 5, the uncertainty in the abundance has been computed by propagating the errors on T_{eff} and $\log g$ and taking into account the standard deviation of the mean obtained from individual determinations in each interval of the analysed spectrum. For elements whose lines occurred in one or two intervals only, the error in the abundance was evaluated by varying the effective temperature and gravity within their uncertainties, $[T_{eff} \pm \delta T_{eff}]$ and $[\log g \pm \delta \log g]$, and computing the abundance for T_{eff} and $\log g$ values in these ranges.

Helium: HD 49606 has already been studied by Catanzaro et al. (1999), for what concern the spectral variability of He I λ5875 Å. These authors concluded that helium is not variable and the λ 5875 Å is weaker than a line belonging to a normal main-sequence star of the same effective temperature. Since helium is underabundant, neutral lines are very difficult to be detected. Among the He I lines we considered the λλ4026, 4120, 4471, 4713, 4921, 5015, 5875, and 6678 Å lines that can be well modelled in local thermodynamic equilibrium (LTE) approximation at the temperature we found for HD 49606 (Leone & Lanzafame 1997, 1998). All these lines are fairly well reproduced by the same abundance, i.e. $\log \frac{He}{N_{tot}} = -2.02 \pm 0.03$. The weakness of all the He I lines observed in HD 49606 may justify the LTE assumption. The evidence that all helium lines are reproduced by the same abundance can be interpreted as due to an uniform distribution throughout the atmosphere.

Carbon: for the carbon abundance reported in Table 3, we used three lines, the C II λ4267.261 Å and the red doublet C II λλ6578.052, 6582.882 Å. All these lines could be reproduced by a solar carbon abundance.

[2] IDL (Interactive Data Language) is a registered trademark of Exelis Visual Information Solutions.

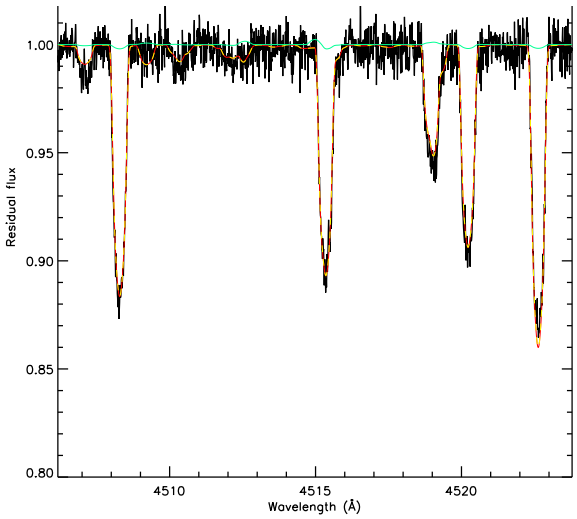

Figure 4. Comparison between observed (HARPS-N@TNG) and synthetic spectra in the range 4506–4524 Å. Synthetic spectra are computed as follows: dashed red line represent spectrum of a single star, dashed yellow line refers to a model for which the contribution of the secondary flux scaled by the radii ratio was considered, and with a green line we represent the ratio between them. For the sake of clarity, this ratio has been multiplied for a factor of 10.

Table 3. Abundances inferred for HD 49606 compared with the solar values from Grevesse et al. (2010). Abundances are expressed in the usual form $\log \frac{N_{el}}{N_{Tot}}$. Sodium abundance has to be intended only as an upper limit.

El	HD 49606	Sun	[HD 49606]
He	-2.02 ± 0.10	-1.13 ± 0.01	-0.92 ± 0.10
C	-3.61 ± 0.22	-3.60 ± 0.05	-0.01 ± 0.23
O	-3.60 ± 0.18	-3.34 ± 0.05	-0.26 ± 0.19
Ne	-3.61 ± 0.13	-4.10 ± 0.10	0.49 ± 0.16
Na	≤ -5.00	-5.79 ± 0.04	≤ 0.79
Mg	-4.57 ± 0.35	-4.43 ± 0.04	-0.55 ± 0.35
Si	-4.48 ± 0.33	-4.52 ± 0.03	-0.02 ± 0.33
P	-4.36 ± 0.26	-6.62 ± 0.03	2.20 ± 0.26
S	-5.56 ± 0.13	-4.91 ± 0.03	-0.65 ± 0.13
Ar	-4.80 ± 0.10	-5.63 ± 0.13	0.83 ± 0.16
Ca	-5.40 ± 0.10	-5.69 ± 0.04	0.29 ± 0.11
Ti	-6.45 ± 0.17	-7.08 ± 0.05	0.63 ± 0.18
Cr	-6.02 ± 0.16	-6.39 ± 0.04	0.37 ± 0.16
Mn	-4.75 ± 0.14	-6.60 ± 0.04	1.85 ± 0.15
Fe	-4.18 ± 0.18	-4.53 ± 0.04	0.35 ± 0.18
Ni	-6.17 ± 0.16	-5.81 ± 0.04	-0.36 ± 0.17
Cu	-6.83 ± 0.13	-7.84 ± 0.04	1.01 ± 0.14
Xe	-4.83 ± 0.22	-9.79 ± 0.06	4.96 ± 0.23
Hg	-6.65 ± 0.25	-10.86 ± 0.08	4.26 ± 0.27

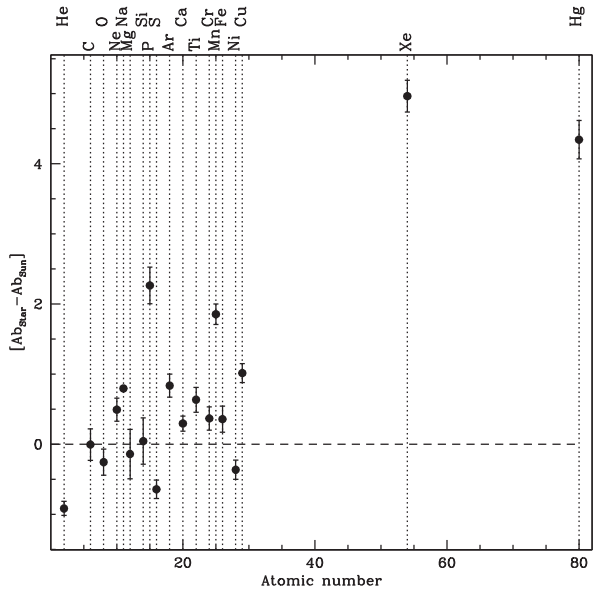

Figure 5. Chemical patterns derived for our target. Horizontal dashed line corresponds to solar abundances (Grevesse et al. 2010).

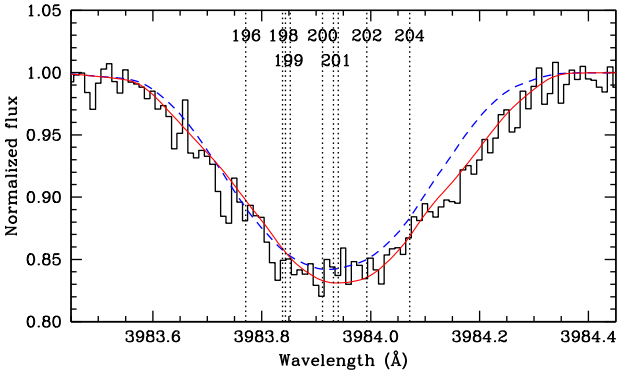

Figure 6. The observed (histogram) line profile of the Hg II λ 3984 Å line is matched (solid red line) with a synthetic line computed with $\log N_{\rm Hg}/N_{\rm tot} = -6.65$ and for the isotopic mixture reported in the text. A blue dashed line represents the synthetic line profile computed for a terrestrial isotopic mixture.

Oxygen: for what concerns oxygen, we have used the triplet at 6155–6158 Å from the EMMI@ESO spectrum and the IR one at 7771–7775 Å from CAOS@OAC. The lines of the red triplet are well reproduced in the LTE approximation by the same abundance, while for IR lines, we used the same approach already discussed in Sitnova, Mashonkina & Ryabchikova (2013), Catanzaro et al. (2015). Since the abundances obtained from the two triplets are consistent within the errors, we adopted their mean value. We obtained an underabundance of 0.26 dex with respect to the Sun.

Neon: eight lines have been used to infer the Ne I abundance: λλ5764.419, 5852.488, 6074.337, 6096.163, 6143.062, 6163.594, 6334.428, 6402.248 Å. The result is an overabundance of ≈0.5 dex with respect to the solar values.

Sodium: by using the doublet at 5890–5895 Å, only an upper limit could be estimated, because of the strong presence of telluric lines.

Magnesium: in our visible spectra, we have only two magnesium lines: the Mg II λ4481 Å and Mg II λ4739.709 Å. From these, we estimated an underabundance of ≈−0.5 dex.

Silicon and phosphorus: for silicon, we found an appreciable discrepancy between abundances derived from Si II lines (−4.50 ± 0.11) and those derived from Si III lines (−4.17 ± 0.03). The same discrepancy and also a greater dispersion around the mean value, has been found for phosphorus. In particular, from P II, we obtained log P II/$N_{\rm tot}$ = − 4.32 ± 0.25, while from P III, we obtained log P III/$N_{\rm tot}$ = − 4.61 ± 0.12. These results have been interpreted by us in terms of vertical stratification along the stellar atmosphere (see discussion in Section 6).

Sulfur: underabundance of about 0.6 dex has been derived by using the line S II λ 4153.068 Å.

Argon: only one line has been detected in our spectra, i.e. Ar II λ 4545.052 Å, from which we obtained an overabundance of ≈0.8 dex.

Calcium: also for calcium only one line has been detected in our spectrum, precisely Ca II λ 5307.224 Å. From this line, we derived an overabundance of about 0.2 dex with respect to the Sun.

Iron-peak elements: moderate overabundances, ≈0.4 dex, of iron and chromium have been inferred from our spectral synthesis, titanium results to be 0.7 dex over the Sun, while about 2 dex is the overabundance inferred from manganese lines. Nickel lines indicate an underabundance of about −0.4 dex. In agreement to Savanov & Hubrig (2003), we did not find sign of chromium stratification.

Copper: lines at λλ4909.734, 4917.892, and 4931.698 Å were observed in our EMMI@NTT spectrum. The deducted abundance is −6.83 ± 0.08, i.e. ≈1 dex over the solar abundance.

Xenon: the xenon content in HD 49606 has also been investigated by using five lines of Xe II, namely at: λλ4603.030, 4844.330, 5292.220, 5419.155, and 5472.601 Å for which wavelengths and oscillators strengths have been reported by Dworetsky et al. (2008) and by Yüce, Castelli & Hubrig (2011). Spectral synthesis of these lines gives an overabundance of xenon, with respect to the solar value, of about 5.0 dex.

Mercury: the only unblended mercury line in our spectra is the Hg II λ 3984 Å, while the other spectral line at λ4358 Å is confused at the level of the continuum.

Usually, mercury in this kind of stars shows a shift due to different isotopic composition, and the line profile can be a blend of seven stable isotopes (A = 196, 198, 199, 200, 201, 202, 204) of which those with odd isotope numbers are further split into hyperfine components, which relative abundances could deviate from the terrestrial mixture. For sake of completeness, the readers are strongly encouraged to see the seminal works by Bidelmann (1966), Dworetsky, Ross & Aller (1970) and Smith (1997) or the more recent application to HgMn stars by Catanzaro, Leone & Leto (2003) and Catanzaro & Leone (2006).

In this study, we took advantage of the highest resolving power of the HARPS-N spectrum to investigate if HD 49606 presents or not isotopic shifts. For this purpose, we proceeded as the following: starting from the terrestrial mixture (dashed blue line in Fig. 6), we changed relative intensities of each isotope (with the requirement that their sum must be equal to unity), until we achieved a good agreement between the observed and synthetic spectral line. Relative intensities thus obtained are multiplied into the total gf value for the line to yield the effective gf values of each of its components. From the perspective of line-profile calculations, this representation is essentially equivalent to treating the mercury isotopes as explicit, distinct species, that contribute to the total line profile. For our calculation, we adopted log gf = −1.520 (Castelli & Hubrig 2004) for the all transitions responsible for the Hg II line. Wavelengths for each isotopic transition and terrestrial isotopic mixture have been

Table 4. Wavelengths, terrestrial and adopted mixtures for mercury lines. Odd components with hyperfine structure are marked with a and b superscripts.

Isotope (A)	Wavelength (Å)	Relative intensity Terrestrial	Adopted
196	3983.769	0.0015	0.0045
198	3983.838	0.1000	0.1800
199[a]	3983.838	0.0714	0.0990
199[b]	3983.849	0.0971	0.0990
200	3983.909	0.2290	0.0300
201[a]	3983.930	0.0480	0.0220
201[b]	3983.941	0.0830	0.0200
202	3983.990	0.3000	0.3000
204	3984.071	0.0700	0.2500

taken from Smith (1997) and reported in Table 4, as well as our adopted mixture. The synthetic (solid red) line shown in Fig. 6 has been computed for $\log N_{\rm Hg}/N_{\rm tot} = -6.65$, that is ≈4.3 dex over the solar value.

6 SEARCH FOR CHEMICAL STRATIFICATION

The analysis reported in the previous sections has raised two important considerations regarding the abundances of silicon and phosphorus: (i) the abundances deduced from the various spectral lines are dispersed around the mean value, and (ii) do exist a significative discrepancy between abundances derived from lines of single and double ionized stages. Moreover, for HD 49606, Leone et al. (1997) have found evidence of magnesium stratification by combining their abundance with those derived from UV lines by Smith (1993).

In this section, we take into account these three elements and we examined the abundances derived for a sample of spectral lines, as a function of the optical depth at λ5000 Å. To relate the line formation to the optical depth, we have computed the contribution function of the line core as in Leone & Lanzafame (1997).

To extend the depth of atmosphere probed by our analysis, we also include four IUE spectra downloaded from MAST archive, two of which have been obtained with the Short-Wavelength Prime camera (SWP: 14965 and 14966), while the two others have been obtained with the Long-Wavelength Redundant camera (LWR: 11522 and 11523). After an accurate check of the flux constancy, we manually co-added all these spectra obtaining a unique spectrum which covers the 1150–3350 Å interval.

In their spectroscopic analysis of HR 6000, Castelli & Hubrig (2007) found phosphorus abundance derived from P II lines greater than that derived from P III lines. They discussed the possible vertical stratification of phosphorus as a possible explanation of the observed discrepancy. For what concerns our target, we analysed the behaviour of the abundances inferred from all the lines reported in Table 5, i.e. 31 lines of P II and 2 lines from P III. The measurements display a bimodal behaviour: an increase of the abundance from ≈100 times solar values at $\log \tau_{5000} \approx 0.00$ up to ≈630 times solar values at $\log \tau_{5000} \cong -2.00$, and a constant abundance of ≈ 100 times solar values in the interval $-5.00 < \log \tau_{5000} < -2.20$ (see Fig. 7).

Silicon stratification in a sample of B-type stars, both normal, magnetic and HgMn, has been studied by Bailey & Landstreet (2013). These authors explored the possibility that the discrepancy observed between Si II and Si III abundances are due to its non-uniform vertical distribution in the atmosphere. They also found that Si II lines result in a larger abundance than that derived from

Table 5. Phosphorus spectral lines selected, with derived abundances and $\log \tau_{5000}$ computed for the line core.

Å	$\log gf$	$\log \frac{N_{\rm P}}{N_{\rm tot}}$	$\log \tau_{5000}$
P II			
1521.659	0.240	−4.50	−2.62
1535.923	− 2.167	−4.50	−4.76
1542.304	− 1.924	−4.46	−4.99
4044.576	0.481	−4.38	−0.79
4127.559	− 0.110	−4.40	−0.58
4420.712	− 0.329	−4.52	−0.97
4452.472	− 0.194	−4.40	−0.52
4463.027	0.026	−4.54	−0.62
4466.150	− 0.560	−4.50	−0.34
4475.270	0.440	−4.62	−0.86
4565.287	− 0.520	−4.47	−0.36
4602.069	0.740	−4.40	−1.16
4626.708	− 0.320	−4.50	−0.52
4658.309	− 0.320	−4.60	−0.52
4927.197	− 0.680	−4.55	−0.40
4935.631	− 0.161	−4.56	−0.43
4943.497	0.060	−4.43	−0.74
4954.367	− 0.542	−4.38	−0.45
5296.077	− 0.160	−4.02	−1.29
5344.729	− 0.390	−4.22	−1.11
5409.722	− 0.390	−4.21	−1.10
5425.880	0.180	−3.95	−1.66
5483.519	− 0.690	−4.29	−0.42
6024.178	0.137	−3.74	−1.69
6034.039	− 0.220	−3.97	−1.33
6043.084	0.416	−3.79	−1.99
6055.504	0.056	−4.30	−0.71
6087.837	− 0.346	−4.05	−1.20
6367.240	− 1.900	−4.49	−0.46
6435.282	− 0.903	−4.43	−0.81
6459.945	0.161	−4.20	−1.65
P III			
4222.198	0.210	−4.52	−0.31
4059.312	− 0.051	−4.70	−0.23

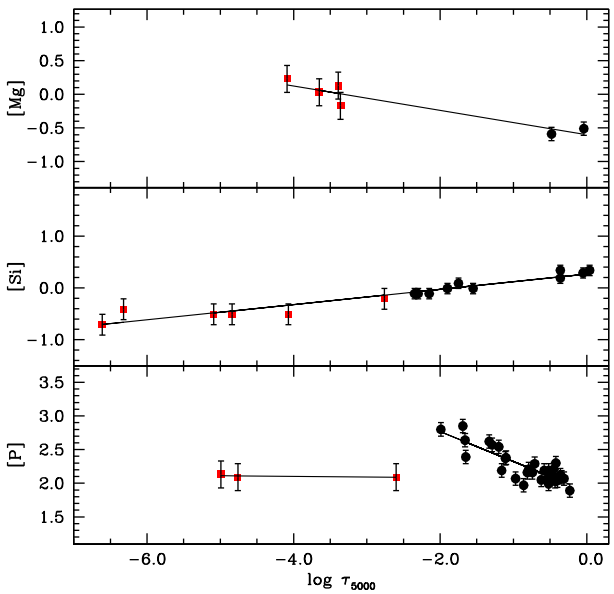

Figure 7. Abundances of phosphorus, silicon and magnesium as a function of optical depth. Red squares represent abundances derived from UV lines, black circles are abundances from optical lines.

Table 6. As Table 5, for silicon spectral lines.

Å	log *gf*	log $\frac{N_{Si}}{N_{tot}}$	log τ_{5000}
Si II			
1526.707	− 0.588	−4.90	−6.32
1533.431	− 0.288	−5.20	−6.61
1711.304	− 0.200	−4.70	−2.76
1808.013	− 2.100	−5.00	−4.84
1816.928	− 1.840	−5.00	−5.09
1817.451	− 2.800	−5.00	−4.07
4128.054	0.359	−4.60	−2.15
4130.894	0.552	−4.60	−2.35
5041.024	0.029	−4.40	−1.75
5055.984	0.523	−4.60	−2.30
5957.559	− 0.225	−4.50	−1.55
5978.930	0.084	−4.50	−1.90
6347.109	0.263	−4.30	−0.36
Si III			0.04
4552.662	0.181	−4.15	
4567.840	0.068	−4.15	−0.36
4574.757	− 0.409	−4.20	−0.05

Table 7. As Table 5, for magnesium spectral lines.

Å	log *gf*	log $\frac{N_O}{N_{tot}}$	log τ_{5000}
2790.777	0.273	−4.20	−4.09
2797.929	− 0.420	−4.60	−3.36
2797.998	0.530	−4.60	−3.36
2928.633	− 0.540	−4.30	−3.39
2936.510	− 0.240	−4.40	−3.65
4481.126	0.749	−5.02	−0.48
4481.150	− 0.553	−5.02	−0.48
4481.325	0.594	−5.02	−0.48
4739.709	− 0.816	−4.94	−0.04

Si III. To verify if this element shows stratification in HD 49606, we derived abundances for the 13 Si II and 3 Si III single lines, reported in Table 6. Similarly to what we did for phosphorus, these abundances have been plotted versus optical depth and showed in Fig. 7. Evidence of stratification has been found also for silicon, in fact it shows a continuous decrement, with larger abundance in the internal layers (mostly derived from Si III lines) of about 2.5 times solar value at $\log \tau_{5000} \cong 0.0$, and it decreases towards external layers to about 0.16 times solar value at $\log \tau_{5000} \cong -6.6$.

For what concern magnesium, we used Mg II λ 4481 Å and Mg II λ 4739.709 Å in the visible range and the UV lines reported in Table 7. As a result, we obtained a non-uniform magnesium abundance, from an almost solar values in the external layers to ≈−0.5 in the deepest layers, see upper panel of Fig. 7.

For these chemical elements, in order to verify if the stratification can be considered real, we have calculated the slope a of the abundances versus $\log \tau_{5000}$ by a linear fit to the data, in the form $\log \frac{N_{el}}{N_{tot}} = a \cdot \log \tau_{5000} + b$. The slope a, the coefficient b and their errors are summarized in Table 8. We required that to be statistically significant in comparison to the experimental errors, the slope a should satisfy the condition $a > 3\sigma$, where σ is its error computed in the fit procedure. As expected, this condition is verified for phosphorus, silicon and magnesium. Further, we computed also the Pearson correlation coefficient between optical depth and abundances, obtaining a positive correlation for silicon, $r = 0.96$, and a negative correlation both for phosphorus, $r = -0.85$ and magnesium, $r = -0.95$ (see the last column of Table 8).

Table 8. Linear coefficient of the lines ($y = ax + b$) represented in Fig. 7. In the last column, we report the Pearson correlation coefficient.

El.	*a*	*b*	*r*
P	− 0.44 ± 0.05	1.88 ± 0.05	− 0.85
Si	0.15 ± 0.01	0.27 ± 0.04	0.96
Mg	− 0.18 ± 0.03	− 0.60 ± 0.10	− 0.95

7 MAGNETIC FIELD

Following the observational strategy described in Leone et al. (2011), to measure the effective magnetic field of HD49606, circular spectropolarimetric observations have been carried out with CAOS@OAC for two consecutive nights on 2015 November 13 and 14. A line-by-line measurement of the effective magnetic field has been attempted as in Leone & Catanzaro (2004) to evidence any possible dependence on element distribution on the stellar surface.

Without any evidence of magnetic field from single spectral lines, we have attempted to combine all Stokes I and V profiles according to the Least-Square Deconvolution (LSD) method (Donati et al. 1997). An upper limit for the field as observed on JD 57339.6 and on JD 57340.6 is $|B_{eff}| < 50$ G.

8 CONCLUSIONS

In this paper, we presented a spectroscopic analysis of the HgMn star HD 49606, based on spectra acquired by us (CAOS, HARPS-N, CASLEO and FRESCO) and also on data retrieved from ESO (EMMI and CES) and CFHT (Gecko) archives. Our purposes were multiple: to investigate if this star shows radial velocity variation due to its membership in a binary system, to identify possible vertical stratification of chemical species and to detect magnetic field, if any.

From our analysis, we derived an orbital motion for our target with a period of 148.30 ± 0.04 d in an eccentric orbit ($e = 0.40 \pm 0.01$) and with a small semi-amplitude ($K = 4.2 \pm 0.4$ km s^{-1}). In all our spectra, we did not find any spectral signature of the secondary component, but using literature data together with the mass function derived by our orbital solution, we estimated its mass in $M_2 = 1.55 \pm 0.20$ M$_\odot$, which corresponds to a star with a spectral type of F1V and a radius $R_2 = 1.45 \pm 0.16$ R$_\odot$.

Abundances have been inferred by spectral synthesis based on ATLAS12 atmospheric model with $T_{eff} = 13\,000 \pm 150$ K, $\log g = 3.80 \pm 0.05$, and $\xi = 0.3^{+0.9}_{-0.0}$ km s^{-1}. Spectral lines broadening are compatible with a $v_e \sin i = 19.0 \pm 0.5$ km s^{-1}. The synthetic spectrum computed by SYNTHE has been compared with observed spectra, in particular for wavelengths shorter than 6500 Å, we used the EMMI spectrum while for longer wavelengths we used our CAOS spectrum. This comparison has shown a complex chemical pattern, with underabundances of helium ([−0.92]), oxygen ([−0.26]), sulfur ([−0.65]), and nickel ([−0.36]), solar composition for carbon and overabundances for all the other elements, in particular manganese ([1.85]), xenon ([4.96]) and mercury ([4.26]). A striking peculiarity is the absence of any overabundances for heavy elements with $Z > 40$, with the exception of xenon and mercury. The same behaviour has been already observed in another puzzling HgMn star, HR 6000 by Catanzaro et al. (2004) and by Castelli & Hubrig (2007).

We found evidences of vertical stratification in the atmosphere of HD 49606 for magnesium, silicon and phosphorus. In the text, we discussed the behaviour of abundances derived from a sample of spectral lines of those elements as a function of optical depth. Those abundances show a strong linear correlation with depth, with a

tendency to float in the upper layers for phosphorus and magnesium, and on the contrary to sink for what that concern silicon.

Two circular spectropolarimetric observations have been carried out to detect magnetic field. No evidence of magnetic field was found by line by line measurements. Applying the LSD technique, we established an upper limit for the absolute value of $B_{\rm eff}$ of about 50 G.

ACKNOWLEDGEMENTS

This paper is partially based on observations made with the Catania Astrophysical Observatory Spectropolarimeter (CAOS) operated by Catania Astrophysical Observatory. This research has made use of the SIMBAD data base, operated at CDS, Strasbourg, France.

This publication makes use of data products from the *WISE*, which is a joint project of the University of California, Los Angeles, and the Jet Propulsion Laboratory/California Institute of Technology, funded by the National Aeronautics and Space Administration.

Based on INES data from the IUE satellite.

Partially based on observations made with ESO Telescopes at the La Silla Paranal Observatory under programme ID 62.L-0348(A) and 68.D-0445(A).

Partially based on observations made with the Italian Telescopio Nazionale Galileo (TNG) operated on the island of La Palma by the Fundación Galileo Galilei of the INAF (Istituto Nazionale di Astrofisica) at the Spanish Observatorio del Roque de los Muchachos of the Instituto de Astrofisica de Canarias.

REFERENCES

Abt H. A., Levato H., Grosso M., 2002, ApJ, 573, 359
Aikman G. C. L., 1976, Publ. Dom. Astrophys. Obs. Victoria, 14, 379
Alecian G., Stift M. J., 2002, A&A, 387, 271
Anderson E., Francis C., 2012, Astron. Lett., 38, 331
Bailey J. D., Landstreet J. D., 2013, A&A, 551, A30
Bidelmann W. P., 1966, in Hubenet H., ed., Proc. IAU Symp. 26, Abundance Determination in Stellar Spectra. Academic Press, London, p. 229
Castelli F., Hubrig S., 2004, A&A, 425, 263
Castelli F., Hubrig S., 2007, A&A, 475, 1041
Catanzaro G., Leone F., 2006, MNRAS, 373, 330
Catanzaro G., Leto P., 2004, A&A, 416, 661
Catanzaro G., Leone F., Catalano F. A., 1999, A&AS, 134, 211
Catanzaro G., Leone F., Leto P., 2003, A&A, 407, 669
Catanzaro G., Leone F., Dall T. H., 2004, A&A, 425, 641
Catanzaro G. et al., 2015, MNRAS, 451, 4703
Chunakova N. M., Bychov V. D., Glagolevskii Yu. V., 1981, Soobshch. Spets. Astrofiffiz. Obs., 31, 5
Cosentino R. et al., 2012, in McLean I. S., Ramsay S. K., Takami H., eds, Proc. SPIE Conf. Ser. Vol. 8446, Ground-based and Airborne Instrumentation for Astronomy IV. SPIE, Bellingham, p. 1
Donati J.-F., Semel M., Carter B. D., Rees D. E., Collier Cameron A., 1997, MNRAS, 291, 658
Drilling J. S., Landolt A. U., 1999, in Cox A. N., ed., Allen's Astrophysical Quantities, 4th edn. Los Alamos. Springer-Verlag, p. 381
Dworetsky M. M., 2004, in Zverko J., Ziznovsky J., Adelman S. J., Weiss W. W., eds, Proc. IAU Symp. 224, The A-Star Puzzle. Kluwer, Dordrecht, p. 727
Dworetsky M. M., Ross J. E., Aller L. H., 1970, BAAS, 2, 311
Dworetsky M. M., Persaud J. L., Patel K., 2008, MNRAS, 385, 1523
Garrison R. F., Gray R. O., 1994, AJ, 107, 1556
Gerbaldi M., Floquet M., Hauck B., 1985, A&A, 146, 341
Glagolevskij J. V., Panov K., Chunakova N. M., 1985, Astronomicheskii Zhurnal, Pisma, 11, 749
Grevesse N., Asplund M., Sauval A. J., Scott P., 2010, Ap&SS, 328, 179
Hauck B., Mermilliod M., 1998, A&AS, 129, 431
Hubrig S., Launhardt R., 1993, ASP Conf. Ser. Vol. 44, IAU Coll. 138, Peculiar versus Normal Phenomena in A-type and Related Stars. Astron. Soc. Pac., San Francisco, p. 350
Hubrig S., North P., Shöeller M., Mathys G., 2006, Astron. Nachr., 327, 289
Ishihara D. et al., 2010, A&A, 514A, 1
Jamar C., Macau-Hercot D., Monfils A., Thompson G. I., Houziaux L., Wilson R., 1976, Ultraviolet Bright Stars Spectrophotometric CATalogue, ESA SR-27
Kurucz R. L., 1993a, in Dworetsky M. M., Castelli F., Faraggiana R., eds, ASP Conf. Ser. Vol. 44, IAU Colloq. 138, A New Opacity-sampling Model Atmosphere Program for Arbitrary Abundances. Astron. Soc. Pac., San Francisco, p. 87
Kurucz R. L., 1993b, Kurucz CD-ROM 13: ATLAS9. SAO, Cambridge
Kurucz R. L., 1997, in Philip A. G. D., Liebert J., Saffer R., Hayes D. S., eds, Model Atmospheres for Individual Stars with Arbitrary Abundances. L. Davis Press, Schenectady, NY, p. 33
Kurucz R. L., Avrett E. H., 1981, SAO Special Report, 391
Kurucz R. L., Bell B., 1995, Kurucz CD-ROM No. 23
Leone F., Catalano F. A., 1991, A&A, 242, 199
Leone F., Catanzaro G., 2004, A&A, 425, 271
Leone F., Lanzafame A. C., 1997, A&A, 320, 893
Leone F., Lanzafame A. C., 1998, A&A, 330, 306
Leone F., Manfrè M., 1997, A&A, 320, 257
Leone F., Catalano F. A., Malaroda S., 1997, A&A, 325, 1125
Leone F., Martínez González M. J., Corradi R. L. M., Privitera G., Manso Sainz R., 2011, ApJ, 731, L33
Leone F. et al., 2016, AJ, 151, 116
Lindroos K. P., 1985, A&AS, 60, 183
McDonald I., Zijlstra A. A., Boyer M. L., 2012, MNRAS, 427, 343
Michaud G., 1970, ApJ, 160, 641
Moon T. T., Dworetsky M. M., 1985, MNRAS, 217, 305
Netopil M., Paunzen E., Maitzen H. M., North P., Hubrig S., 2008, A&A, 491, 545
Pasinetti Fracassini L. E., Pastori L., Covino S., Pozzi A., 2001, A&A, 367, 521
Paunzen E., Wraight K. T., Fossati L., Netopil M., White G. J., Bewsher D., 2013, MNRAS, 429, 119
Pickles A., Depagne E., 2010, PASP, 122, 1437
Preston G. W., 1974, ARA&A, 12, 257
Renson P., Gerbaldi M., Catalano F. A., 1991, A&AS, 89, 429
Savanov I, Hubrig S., 2003, A&A, 410, 299
Schöeller M. S., Correia S., Hubrig S., Ageorges N., 2010, A&A, 522, 85
Sitnova T. M., Mashonkina L. I., Ryabchikova T. A., 2013, Astron. Lett., 39, 126
Smith K. C., 1993, A&A, 273, 393
Smith K. C., 1996, Ap&SS, 237, 77
Smith K. C., 1997, A&A, 319, 928
Spanò P., Leone F., Scuderi S., Catalano S., Zerbi F., 2004, in Moorwood A. F. M., Masanori I., eds, Proc. SPIE Conf. Ser. Vol. 5492, Ground-based Instrumentation for Astronomy. SPIE, Bellingham, p. 373
Spanò P., Leone F., Bruno P., Catalano S., Martinetti E., Scuderi S., 2006, Mem. Soc. Astron. Ital. Suppl., 9, 481
Stickland D. J., Weatherby J., 1984, A&AS, 57, 55
Stift M. J., Alecian G., 2016, MNRAS, 457, 74
Thompson G. I., Nandy K., Jamar C., Monfils A., Houziaux L., Carnochan D. J., Wilson R., 1978, 'Catalogue of stellar ultraviolet fluxes (TD1): A compilation of absolute stellar fluxes measured by the Sky Survey', The Science Research Council
Van Leeuven F., 2007, A&A, 474, 653
Vauclair S., 1975, A&A, 45, 233
Wright E. L. et al., 2010, AJ, 140, 1868
Yüce K., Castelli F., Hubrig S., 2011, A&A, 528, A37

This paper has been typeset from a TEX/LATEX file prepared by the author.